# Fresnel zone plate stacking in the intermediate field for high efficiency focusing in the hard X-ray regime

**Sophie-Charlotte Gleber,[1,*] Michael Wojcik,[1] Jie Liu,[1] Chris Roehrig,[1] Marvin Cummings,[1] Joan Vila-Comamala,[1,2] Kenan Li,[3] Barry Lai,[1] Deming Shu,[1] and Stefan Vogt[1]**

[1]*Argonne National Laboratory, 9700 S Cass Ave, Argonne, Il 60439 USA*
[2]*current address: Diamond Light Source Ltd, Harwell Science and Innovation Campus, Didcot - Oxfordshire OX11 0DE United Kingdom*
[3]*Northwestern University, 633 Clark St, Evanston, Il 60208 USA*

[*]*gleber@aps.anl.gov*

**Abstract:** Focusing efficiency of Fresnel zone plates (FZPs) for X-rays depends on zone height, while the achievable spatial resolution depends on the width of the finest zones. FZPs with optimal efficiency and sub-100-nm spatial resolution require high aspect ratio structures which are difficult to fabricate with current technology especially for the hard X-ray regime. A possible solution is to stack several zone plates. To increase the number of FZPs within one stack, we first demonstrate intermediate-field stacking and apply this method by stacks of up to five FZPs with adjusted diameters. Approaching the respective optimum zone height, we maximized efficiencies for high resolution focusing at three different energies, 10, 11.8, and 25 keV.



**OCIS codes:** (340.0340 ) X-ray optics; (340.7460 ) X-ray microscopy; (340.6720) Synchrotron radiation; (340.7480) X-rays; (050.1965) Diffractive lenses.

## References and links

1. G. Schmahl and D. Rudolph, "Lichtstarke Zonenplatten als abbildende Systeme für weiche Röntgenstrahlen," Optik **29**, 577–585 (1969).
2. B. Niemann and D. Rudolph and G. Schmahl, "Soft x-ray imaging zone plates with large zone numbers for microscopic and spectroscopic applications," Opt. Commun. **12**, 160 (1974).
3. J. Kirz, "Phase zone plates for x rays and the extreme uv," J. Opt. Soc. Am. **64**, 301–309 (1974).
4. J. Kirz and C. Jacobsen and M. Howells, "Soft X-ray microscopes and their biological applications," Q. Rev. Biophys. **28**, 33–130 (1995).
5. T. Paunesku, S. Vogt, J. Maser, B. Lai, and G. Woloschak, "X-ray fluorescence microprobe imaging in biology and medicine," J. Cell Biochem. **99**(6) 1489–1502 (2006).
6. S. Bohic, M. Cotte, M. Salomé, B. Fayard, M. Kuehbacher, P. Cloetens, G. Martinez-Criado, R. Tucoulou, and J. Susini, "Biomedical applications of the ESRF synchrotron-based microspectroscopy platform," J. Struct. Biol. **177**(2) 248–258 (2012).
7. E. Lombi, M. D. de Jonge, E. Donner, C. G. Ryan, and D. Paterson, "Trends in hard X-ray fluorescence mapping: environmental applications in the age of fast detectors", Anal. Bioanal. Chem. **400**(6) 1637–1644 (2011).
8. P. A. C. Jansson, U. Vogt, and H. M. Hertz, "Liquid-nitrogen-jet laser-plasma source for compact soft x-ray microscopy," Rev. Sci. Instrum. **76** 43503-1-5 (2005).
9. D. Attwood and T. David, *Soft X-rays and Extreme Ultraviolet Radiation: Principles and Applications* (Cambridge University Press, 2000).
10. W. Chao, B. D. Harteneck, J. A. Liddle, E. H. Anderson, and D. T. Attwood, "Soft X-ray microscopy at a spatial resolution better than 15 nm," Nature **435**(7046) 1210–1213 (2005).

#212663 - $15.00 USD Received 5 Jun 2014; revised 8 Aug 2014; accepted 13 Aug 2014; published 5 Nov 2014

11. W. Chao, J. Kim, S. Rekawa, P. Fischer, and E. H. Anderson, "Demonstration of 12 nm resolution Fresnel zone plate lens based soft x-ray microscopy," Opt. Express **17** (20) 17669–17677 (2009).
12. J. Vila-Comamala, S. Gorelick, E. Färm, C. M. Kewish, A. Diaz, R. Barrett, V. A. Guzenko, M. Ritala, and Christian David, "Ultra-high resolution zone-doubled diffractive X-ray optics for the multi-keV regime," Opt. Express **19**(1) 175–184 (2011).
13. S. Gorelick, J. Vila-Comamala, V. A. Guzenko, R. Barrett, M. Salomé, and C. David,"High-efficiency Fresnel zone plates for hard X-rays by 100 keV e-beam lithography and electroplating," J. Synchrotron Rad. **18**(3) 442–446 (2011).
14. M. J. Wojcik, D. C. Mancini, R. Divan, and L. E. Ocola , "X-ray zone plates with 25 aspect ratio using a 2-$\mu m$-thick ultrananocrystalline diamond mold," Microsyst. Technol., 1–6 (2014)
15. J. Vila-Comamala, S. Gorelick, V. A. Guzenko, E. Färm, M. Ritala, and C. David,"Dense high aspect ratio hydrogen silsesquioxane nanostructures by 100 keV electron beam lithography," Nanotechnology **21**(28) 285305 (2010).
16. E. Chubarova, D. Nilsson, M. Lindblom, J. Reinspach, J. Birch, U. Vogt, H. M. Hertz, and A. Holmberg, "Platinum zone plates for hard X-ray applications," Microelectron. Eng. **88**(10) 3123–3126 (2011).
17. B.L. Henke, E.M. Gullikson, and J.C. Davis, "X-ray interactions: photoabsorption, scattering, transmission, and reflection at E=50-30000 eV, Z=1-92," Atom. Data Nucl. Data **54**, 2, 181–342 (1993).
18. A.G. Michette, *Optical Systems for Soft X Rays*, (Plenum Press, 1986).
19. J. Maser, B. Lai, W. Yun, S.D. Shastri, Z. Cai, W. Rodrigues, S. Xu, and Trackhtenberg, "Near-field stacking of zone plates for hard x-ray range," Proc. of SPIE **4783**, 74–81 (2002).
20. I. Snigireva, A. Snigirev, V. Kohn, V. Yunkin, M. Grigoriev, S. Kuznetsov, G. Vaughan, and M. Di Michiel, "Focusing high energy X-rays with stacked Fresnel zone plates," Phys. Sta. Sol. (a) **204** 2817–2823, (2007).
21. Y. Feng, M. Feser, A. Lyon, S. Rishton, X. Zeng, S. Chen, S. Sassolini, and W. Yun, "Nanofabrication of high aspect ratio 24nm x-ray zone plates for x-ray imaging applications," J. Vac. Sci. Technol. B **25** 2004 (2007)
22. S. Werner, S. Rehbein, P. Guttman, S. Heim, and G. Schneider, "Towards stacked zone plates," J. Phys.: Conf. Ser. **186** 012079–012081(2009).
23. I. Mohacsi, P. Karvinen, I. Vartiainen, V.A. Guzenko, A. Somogyi, C.M. Kewish, P. Mercere, and C. David, C., "High-efficiency zone-plate optics for multi-keV X-ray focusing," J. Synchotron Rad. **21**, 497–501 (2014).
24. J. Vila-Comamala, M. Wojcik, A. Diaz, M. Guizar-Sicairos, C.M. Kewis, S. Wang, and C. David, "Angular spectrum simulation of X-ray focusing by Fresnel zone plates," J. Synchrotron Rad. **20**, 397–404 (2013).
25. S. Gorelick, V. A. Guzenko, J. Vila-Comamala, and C. David, " Direct e-beam writing of dense and high aspect ratio nanostructures in thick layers of PMMA for electroplating ," Nanotechnology **21**, 295303 (2010).
26. M. Lu, D. M. Tennant, and C. Jacobsen, "Orientation dependence of linewidth variation in sub-50-nm Gaussian e-beam lithography and its correction," J. Vac. Sci. Technol. B **24**, 2881–2885 (2006).
27. M. Guizar-Sicairos and J. Gutierrez-Vega, "Computation of quasi-discrete Hankel transforms of integer order for propagating optical wave fields," J. Opt. Soc. Am. A **21**, 53–58 (2004).

## 1. Introduction

High-resolution X-ray microscopy began with the fabrication of Fresnel zone plates (FZPs) as diffractive optics suitable for focusing light in the X-ray regime [1–3]. The capability to penetrate relatively thick specimens and provide contrast for absorption, phase, and fluorescence imaging with finer resolution than visible light are the primary reasons X-ray microscopy is a powerful complementary technique within the suite of microscopy techniques (e.g., [4–7]).

In soft X-ray regime, there have been developments of so-called table-top, laboratory-scale, or compact instruments based on laser-plasma X-ray sources for X-ray microscopy [8]. However, due to the requirements of high brilliance or high flux many of the X-ray microscopes are located at synchrotrons sources. The low efficiency of high resolution FZPs limits the flux of photons in the focal spot noticeably even for the high flux provided by synchrotron sources. X-ray imaging techniques, for example hard X-ray fluorescence microscopy, are often limited by the amount of focused photons and an increase of FZP efficiency is one solution to the problem of limited flux. The benefit for higher efficiency zone plates is decreased exposure time enabling better and faster experiments. Focusing efficiency strongly depends on the incident energy [3, 9] and efficiencies typically are below 10 %, though can achieve greater than 20 % efficiency when close to the optimum zone plate thickness for the incident X-ray energy. Depending on the outermost zone width, FZPs have provided a focus of several nm in the soft X-ray regime [10, 11] and few tens of nanometers in the hard X-ray regime [12]. The combi-

#212663 - $15.00 USD Received 5 Jun 2014; revised 8 Aug 2014; accepted 13 Aug 2014; published 5 Nov 2014

nation of high resolution and efficiency are difficult for FZP to reach the theoretical maximum values due to fabrication limitations.

Zone plate efficiency can be at the least approximated by using the efficiency calculation by Kirz *et al.* [3]. For example the efficiency of a gold zone plate in the 5-25 keV energy range is plotted in Fig. 1. The contour lines show calculated efficiencies versus incident energy and FZP thickness. To compare easily with the experimental results presented below, efficiency versus FZP thickness is extracted for the three energies and plotted in Fig. 2. The primary reason for low efficiency for available FZPs with sub-100-nm focus spot size is the limited aspect ratio (zone height over zone width) due to limitations in fabrication methods. Fabrication method will usually result in a zone plate with an aspect ratio of around 10 and occasionally up to 20 [13–16]. The focusing efficiency of hard X-ray zone plates utilized in this paper were in the same range with around 10 % at 10 keV with 80 nm outermost zone width (see Table 1), which was far from ideal. A method to increase the focusing efficiency is to stack several zone plates thereby increasing zone height.

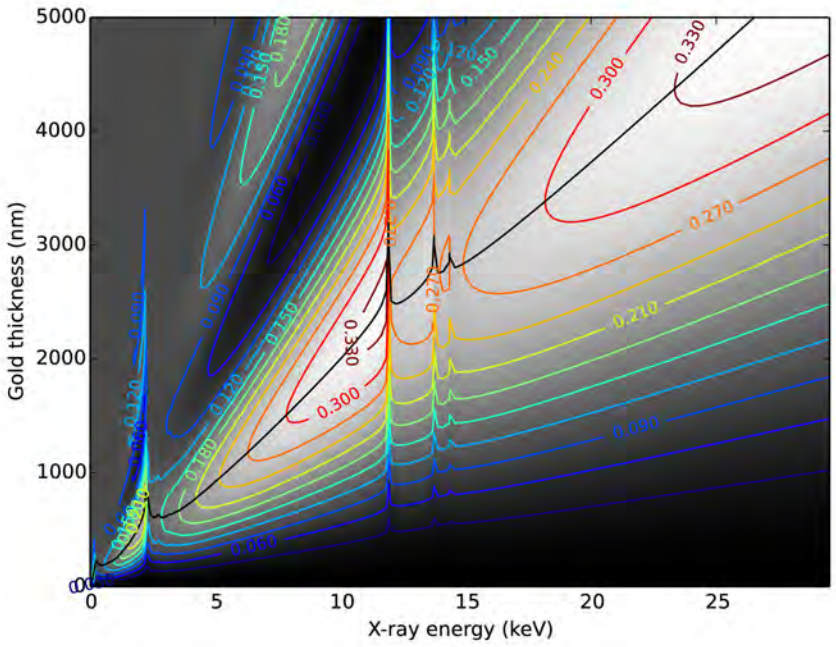


Fig. 1. Plot of zone plate efficiency (isolines) versus zone plate thickness and X-ray energy. Calculated using efficiency calculation in [3] with constants in [17].

## 2. Zone plate stacking

The problem of low efficiency at hard X-rays for zone plates can be addressed through zone plate stacking. The concept is based on achieving an optimum structure height through two or more zone plates perfectly aligned on top of each other and thus acting like one FZP with the total structure height of the stack. If there were a method of placing any number of zone plates to stack on other zone plates, then an optical system can be created to focus X-rays with good efficiency and nanometer spot size. The challenge in this method is to engineer a solution to

#212663 - $15.00 USD Received 5 Jun 2014; revised 8 Aug 2014; accepted 13 Aug 2014; published 5 Nov 2014

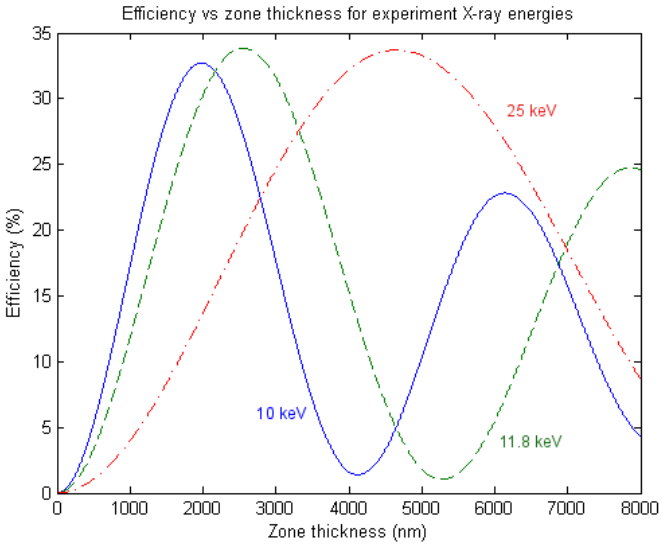


Fig. 2. Plot of zone plate efficiency versus zone plate thickness at three different energies, matching the energies discussed under Results (table 1 and 2).

align multiple zone plates with very high precision. The conditions for alignment for standard stacking are lateral and proximity conditions. The lateral condition is described in Eq. (1) [18] and applies for all cases of zone plate stacking discussed in this paper:

$$\delta < \frac{1}{3} dr_n \tag{1}$$

where $dr_n$ is the outer zone width of a FZP.

However, the proximity condition (Eq. (2)) as introduced below applies only for near-field stacking of similar FZPs. There is another stacking method, in the intermediate field, which has to satisfy the longitudinal condition, but is flexible in the proximity. Both stacking methods are discussed in the following, and first experimental results for the intermediate-field stacking of FZPs are presented.

*Near-field zone plate stacking*

Stacking FZPs involves aligning two optics with the same diameter and outermost zone width in near contact. The zone plates must meet the longitudinal condition as well as the proximity condition presented in Eq. (2) [19]:

$$p < 0.76 \frac{dr_n^2}{\lambda} \tag{2}$$

where $p$ is the distance between the stacked zone plates along the X-ray beam. This implies that the stacked FZPs must be at least as close as roughly 40 % of the depth of focus of the zone plates. For typical depths of focus of 100-200 $\mu m$ this results in a maximum distance of 40-80 $\mu m$ between stacked FZPs.

If both of those alignment conditions (Eqs. (1) and (2)) are met, the stacked zone plates can be considered as a single thin optic. Several examples of stacking zone plates in the near-field have been shown before. Maser *et al.* [19] demonstrated mechanical stacking of two FZPs in the

#212663 - $15.00 USD Received 5 Jun 2014; revised 8 Aug 2014; accepted 13 Aug 2014; published 5 Nov 2014

near-field using separate mounts for each FZP and brought them in a close-to-contact distance to comply with the proximity condition (Eq. (2)). Snigireva *et al.* [20] published a different approach where they created a stack of two FZPs glueing one on top of the other. Feng *et al.* [21] created optical systems with two bonded FZPs with 24 nm outermost zone width. Werner *et al.* [22] showed a slightly different approach where the FZPs to be stacked were fabricated subsequently directly on top of each other. I. Mohacsi *et al.* [23] combined on-chip fabrication with mechanical stacking, where two zone plates, a single and a two on-chip layers one, were stacked in the near-field. Both Werner *et al.* [22] and I. Mohacsi *et al.* [23] expanded the approach of stacking towards volumetric effects achieved by stacking non-similar zone plates. Werner *et al.* [22] approximated an ellipsoidal shaped zone plate for increased efficiency in soft X-ray focusing. For increased efficiency for phase-shift based focusing of hard X-rays, I. Mohacsi *et al.* [23] applied a stepped profile to create a combined zone plate close to a wrapped parabolic lens.

However, on-chip fabrication is complicated due to limitations in aligning subsequent fabrication processes. On the other hand, mechanical stacking of more than two high resolution FZPs is almost inhibited by the proximity condition (Eq. (2)). The barrier preventing mechanical stacking of multiple FZPs mainly consists in support structures like the silicon frame that supports the membrane on which FZPs are fabricated. The silicon frame is typically 250-500 $\mu m$ thick and this makes it difficult to stack three zone plate samples so that each are within the depth of focus limitation along the beam axis. Therefore, to stack mechanically more than two zone plates, a different stacking paradigm must be used.

*Intermediate-field zone plate stacking*

To avoid the challenges of the proximity condition for near-field stacking of identical zone plates, Vila-Comamala *et al.* [24] introduced the idea of stacking FZPs at larger distances. This is possible by adjusting the diameter of the downstream FZP so that its focal length is equal to the focal length of the upstream FZP minus the distance between both FZPs. Thus, the focal spots of both FZPs overlay when the separation of both FZPs is matching the difference in focal lengths. According to their simulations such stack of adjusted diameter FZPs reaches the same efficiency as a stack of two similar FZPs stacked within the proximity conditions. We verified these simulations experimentally and present first results of intermediate-field zone plate stacking in the following.

## 3. Zone plate stacking apparatus

Two different types of FZP stacking apparatuses were used (Shu et al., ANL-IN-13-092). One design, the Z2-34 (Fig. 3(a)) was developed and utilized for the stacking of 3 FZPs in the intermediate field. As shown in Fig. 3(b), the Z2-34 alignment apparatus has a non-symmetric base structure and six commercial piezo-motor-driven linear stages (such as SmarActTM SLC-1720S and PITM LPS-24 stages). They allow for relative travel ranges of several mm in x, y and z between three chips of FZPs with a precision of less than 10 nm as required for lateral alignment (Eq. (1)) of typical FZPs. Each FZP chip is mounted on a 200 $\mu m$ thick CVD-diamond holder. Since the thermal expansion coefficient of CVD diamond is similar to that of invar, it ensures thermal stability of the apparatus. Therefore, relative drift between the stacked zone plates was minimized.

The second apparatus used was the Z2-37 (Fig. 4(b)). Its design is conceptually similar to the Z2-34, but capable of intermediate-field stacking of up to 6 FZPs on a symmetric hexagonal base. For both set-ups, FZPs were fabricated in-house as described in the following section.

#212663 - $15.00 USD Received 5 Jun 2014; revised 8 Aug 2014; accepted 13 Aug 2014; published 5 Nov 2014

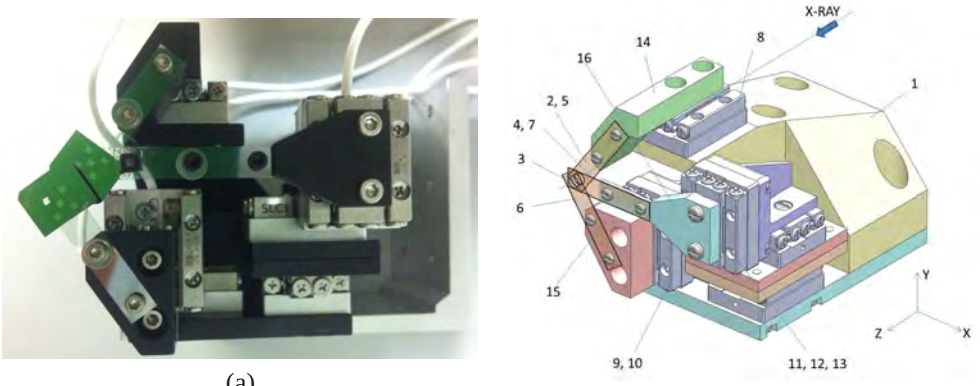


(a) (b)

Fig. 3. The ANL Z2-34 zone plate stacking apparatus. **(a):** Picture of the ANL Z2-34 zone plate stacking apparatus. Three in-house fabricated arrays of Fresnel zone plates are mounted on 200 $\mu m$ thick diamond holders. For positioning of the setup at the beam line, zone plate arrays are initially moved apart as shown here. **(b):** A 3-D model of the Z2-34 precision alignment apparatus for intermediate-field stacking of three zone plates : (1) non-symmetric invar base structure; (2-4) zone plates; (5-7) CVD-diamond holders; (8) Z-stage; (9, 10) X-Y-stages; (11-13) X-Y-Z-stages; (14-16) linkage components. [D. Shu, J. Liu, S. C. Gleber, J. Vila-Comamala, B. Lai, J. Maser, C. Roehrig, M. J. Wojcik, and S. Vogt, U. S. Patent application in progress for ANL-IN-13-092.]

## 4. Zone plate fabrication

Stacked zone plates were fabricated by electroplating Au into a dielectric mold which is subsequently removed. The fabrication process was based on the method presented by Gorelick *et al.* [25] while the zone plate patterns were generated by custom code designed for zone plate fabrication [26]. Every stacked zone plate had an 80-nm-outer most zone width and zone thickness at least 800 *nm* and up to 900 *nm*. Fabricated zone plates were designed with adjusted diameter for intermediate stacking with knowledge of X-ray energy and intermediate stacking distance. The base zone plate had a diameter of 150 $\mu m$ and the other zone plates had diameters to match separation distances of 300 and 1000 $\mu m$ at 10 keV and respectively 500, 1750, 2750 and 3250 $\mu m$ at 25 keV X-ray energy. The base zone plate was set to be the most downstream of the stacked zone plates. The zone plate for 300 $\mu m$ intermediate stacking distance at 10 keV is shown in Fig. 5: The outer zones are visible in Fig. 5(c), and 800-nm-zone thickness is visible in Fig. 5(d), with consistent over the whole zone plate (Fig. 5(a) and (b)).

## 5. Results and discussion

The Z2-34 FZP stacking apparatus was implemented at the hard X-ray microprobe at the 2-ID-E beamline of the Advanced Photon Source. The components crucial for the results presented here are a 150 $\mu m$ upstream pinhole restricting the illumination to the area of the 150 $\mu m$ FZPs, an upstream ion chamber to monitor the flux incident on the FZPs, a central stop blocking the direct beam, the Z2-34 FZP stacking apparatus mounted on an x-y-z stage, a 30 $\mu m$ tungsten pinhole (order sorting aperture, OSA) at about 10 % of the focal length upstream of the focus to select the first diffraction order and block direct light and higher diffraction orders, a downstream ion chamber at about a focal length downstream of the focal spot, and a scintillator crystal with a zoom lens and a charge-coupled device (CCD) to visualize the transmission signal. When the OSA is moved out of the beam, the CCD provides an approximately 1 *mm* wide view on

#212663 - $15.00 USD Received 5 Jun 2014; revised 8 Aug 2014; accepted 13 Aug 2014; published 5 Nov 2014

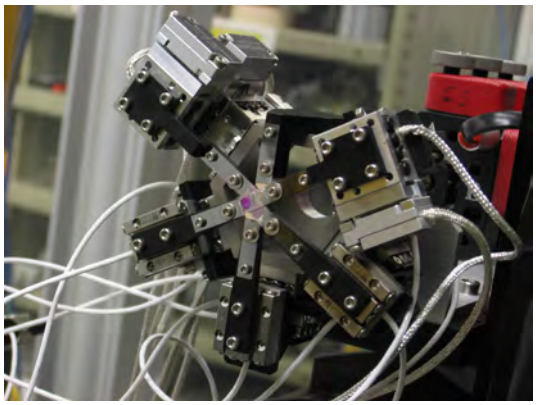

Fig. 4. Picture of the ANL Z2-37 precision alignment apparatus for intermediate-field stacking of up to six zone plates. In-house fabricated arrays of Fresnel zone plates are mounted on diamond holders. The apparatus is shown as integrated to the microprobe setup. [D. Shu, J. Liu, S. C. Gleber, J. Vila-Comamala, B. Lai, J. Maser, C. Roehrig, M. J. Wojcik, and S. Vogt, U. S. Patent application in progress for ANL-IN-13-092]

the scintillator crystal where FZPs and other components can be seen in the transmitted X-ray beam. The focal spot determines the sample position which is within a helium chamber. The fluorescence detector (Vortex ME-4, SII NanoTechnology USA Inc., Northridge, CA, USA) is at 90 degree to the incident beam. Three chips of FZPs as described above were mounted to the apparatus on the diamond holders (Fig. 3). The motors were controlled via the software package EPICS (Argonne National Laboratory, Argonne, IL, USA) and the long travel ranges allowed for the straight forward alignment of all three matching FZPs as described in the following.

In Fig. 6, two steps of the alignment of three FZP with the Z2-34 alignment apparatus is shown. In the transmission image from the CCD, on each FZP chip the dedicated FZP was identified and aligned to a common reference point, marked by the green cross hair visible on the CCD image. While all FZP chips are already in the incident X-ray beam, first the selected upstream and center FZPs get aligned (Fig. 6(a)). The central stop is visible in this alignment as dark spot also centered to the reference point. Once those two FZPs are aligned, the selected FZP on the downstream FZP chip gets moved into the line of stacked FZPs (Fig. 6(b)). In the picture shown, the downstream FZP is only close to alignment, so Moiré fringes are visible. Those fringes are an indication for the alignment, and with all 3 FZPs aligned, the fringes disappear and the transmission image of the stack looks like the one with the 2 FZPs aligned (Fig. 6(a)). For this alignment, the relatively large travel range of the stacking apparatus of several millimeters for each FZP chip was crucial. It allowed for subsequently moving each FZP chip into the beam and identifying the specific FZP for stacking within the array as the entire array could be scanned.

Misalignment of one FZP in the stack becomes not only visible in the form of Moiré fringes in the transmission image (Fig. 6), but also in a decrease of focused flux (measured as decrease of counts in the downstream ion chamber) as the focusing efficiency decays with misalignment. To measure the influence of misalignment, two data sets were acquired. The influence of lateral misalignment was measured moving the central zone plate (CZP) out of alignment in horizontal (x) direction. The step size was 10 *nm* in the region close to alignment and 50 *nm* in the region of more than 350 *nm* away from alignment. For each point the focused flux was measured and converted to FZP efficiency. The resulting plot of FZP efficiency as a function of the lateral alignment of the stacked FZPs is shown in blue in Fig. 7(a). According to the lateral alignment

#212663 - $15.00 USD Received 5 Jun 2014; revised 8 Aug 2014; accepted 13 Aug 2014; published 5 Nov 2014

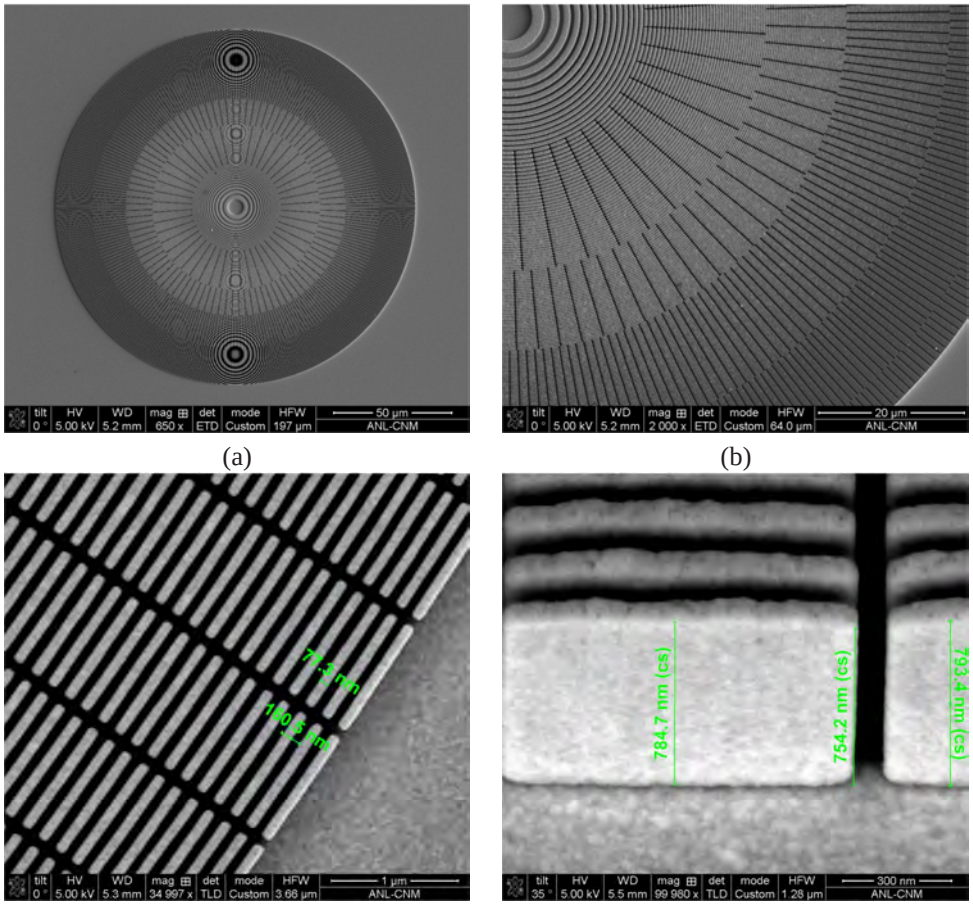


Fig. 5. SEM images of the in-house fabricated Fresnel zone plate used for the 300 $\mu$m separation distance in the stack of three FZPs. Zones were fabricated close to ideal duty cycle and consistent over the whole zone plate (**a** and **b**). The outer zones are visible in **(c)**, and 800-nm-zone thickness is visible in **(d)**.

#212663 - $15.00 USD Received 5 Jun 2014; revised 8 Aug 2014; accepted 13 Aug 2014; published 5 Nov 2014

condition (Eq. (1)), the FZPs we used here should be within 27 *nm*. In good agreement, the plot shows that the efficiency drops noticeably with a lateral misalignment of 30 *nm*.

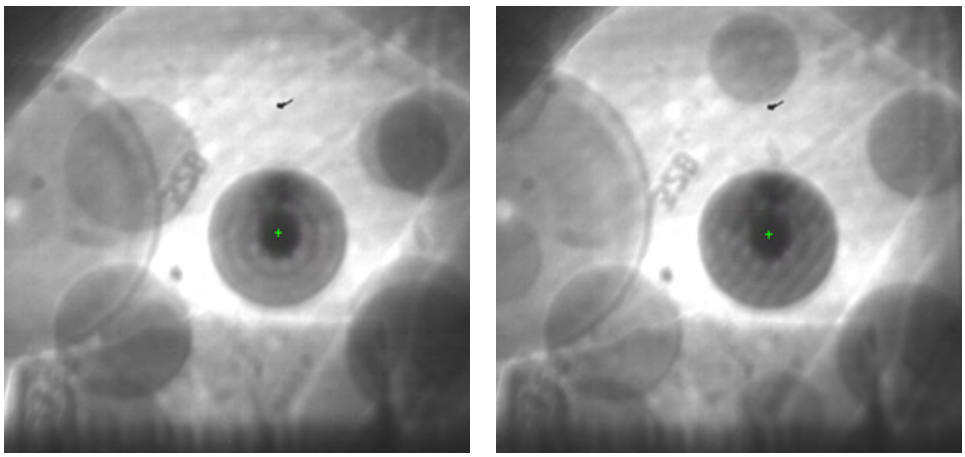

(a) (b)

Fig. 6. Transmission images on the scintillator crystal showing the consecutive alignment of the three chips with arrays of FZPs. While all chips are already in the beam, matching upstream and center FZP get aligned first (**(a)**), centered towards the green dot indicating the reference point on the CCD. The central beam stop is also visible in this alignment. Then, the matching downstream FZP is moved into the line of stacked FZPs. Before final tweaking, the downstream FZP is only close to alignment, creating Moiré fringes (**(b)**).

The influence of longitudinal misalignment, i.e. misalignment along the z axis away from the required proximity of the stacked FZPs, is shown in blue in Fig. 7(b). The measurement was performed by increasing the distance of the downstream FZP out of the optimum position for the intermediate field stacking of the 3 FZPs in steps of 50 $\mu m$. FZP efficiency is plotted versus the longitudinal misalignment of the stacked FZPs. It needs to be pointed out that for near-field stacking, this plot would represent the proximity condition (Eq. (2)) and imply that the zone plates have to be as close as 50 $\mu m$ to avoid efficiency loss. However, here the range of 50 $\mu m$ refers to moving out of the longitudinal alignment distance which was already 300 $\mu m$ between the stacked zone plates. Thus, for intermediate-field stacking the zone plate needs to be positioned within a range given by the proximity condition around the optimum distance, which is dependent on the stacked zone plate parameters and can be several hundreds of micrometers.

Stacked zone plate misalignment in the lateral and beam direction was simulated with an angular spectrum propagation method [24] using a quasi-descrete Hankel transform algorithm **??**. The simulation was tailored to approximate the setup used for experimental data presented in green in Fig. 7, and the drop in efficiency between simulation and experimental data correlated well in the beam axis misalignment Fig. 7(a) but not as well for lateral misalignment Fig. 7(b). However, the cut-off for misalignment is for both the simulated and experimental values around 30 *nm* and thus in good agreement with the lateral alignment condition (Eq. (1)).

With the stacking apparatuses, FZPs could be used individually, and the efficiencies of single and combined FZPs were determined. For efficiency measurements, the flux hitting the FZPs was measured by the downstream ion chamber with a 150 $\mu m$ upstream pinhole and a central beam stop in place and all FZPs moved out of the beam. Then single or stacked FZPs were moved into the beam defined by a 150 $\mu m$ upstream pinhole and the flux in the focus spot was measured in the downstream ion chamber. With the Z2-34, measurements were performed

#212663 - $15.00 USD Received 5 Jun 2014; revised 8 Aug 2014; accepted 13 Aug 2014; published 5 Nov 2014

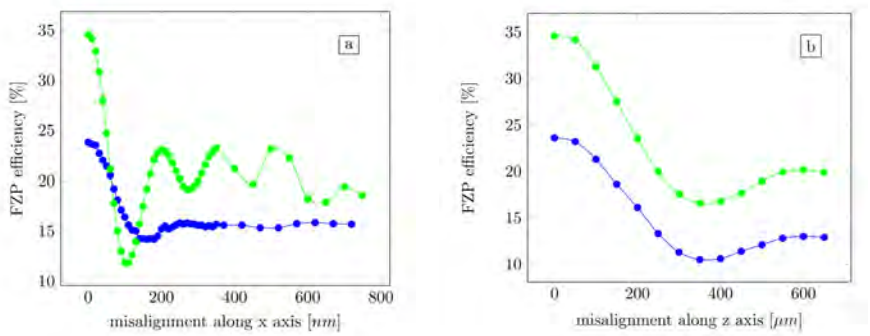


Fig. 7. Efficiency decrease due to misalignment at 11.8 keV, experimental (blue) and simulated (green) values. **(a):** Plot of the efficiency as a function of the lateral alignment of the stacked FZPs. The measurement was performed by moving the center FZP out of alignment in x direction. The step size is 10 *nm* in the region close to alignment and 50 *nm* in the region of more than 350 *nm* misalignment. **(b):** Plot of the efficiency as a function of the longitudinal alignment of the stacked FZPs. The measurement was performed by increasing the distance of the downstream FZP out of the optimum position for the intermediate field stacking of the 3 FZPs in steps of 50 $\mu m$.

under two different incident energies, 10 keV and 11.8 keV to address the energy dependence of efficiency and optimum structure thickness. The structure thickness of individual and combined FZPs as well as resulting efficiencies for both incident energies are presented in Table 1. The values are in good agreement with the theoretical efficiencies also included in the table. For 10 keV incident energy, the optimum structure height is 1.99 $\mu m$. For the combination of FZPs in this experiment, the structure height closest to the optimum height is the stack of DSZP and CZP, resulting in a total height of 1.7 $\mu m$. Accordingly, this combination achieves the best efficiency for 10 keV incident energy, and as expected the stack of 3 FZPs shows less efficiency as its total height of 2.5 $\mu m$ exceeds the optimum height significantly (refer to efficiency plot shown in Fig. 2). However, for 11.8 keV incident energy, the optimum height is 2.55 $\mu m$, thus close to the total height of the stack of 3 FZPs. This is reflected in the measured efficiency of 23.6 % of the 3 FZPs stack, which is higher than the efficiencies for single or stacks of 2 FZPs at that energy. In addition, the focus size in vertical direction was measured as FWHM (full width half maximum) of error functions fitted to line scans over a chromium knife edge for single and combined FZPs. Values achieved at 11.8 keV are presented in Table 1 and show good consistency for single and stacked FZPs.

To underline the extent of efficiency increase by multiple FZP stacking at even higher energy, the Z2-37 was utilized for multiple zone plate stacking at 25 keV. The efficiencies of single and stacked FZPs were measured and are presented together with theoretical values in Table 2. At 25 keV, a single zone plate had a measured efficiency of 2.4 %, which increased almost by a factor of 8 to 19 % when using a stack of 5 zone plates. The measured values follow the progress of the theoretical values, but are expected to improve with further optimized thermal stability of the stacking setup. Also the focus spot sizes measured for single and stacked FZPs are consistent up to four stacked FZPs, but widens slightly with the stack of five.

## 6. Conclusions

We have successfully demonstrated stacking of multiple zone plates in the intermediate field. While for near-field stacking, similar zone plates used would have required a maximum dis-

#212663 - $15.00 USD Received 5 Jun 2014; revised 8 Aug 2014; accepted 13 Aug 2014; published 5 Nov 2014

Table 1. Theoretical (T) and measured (M) values for FZP efficiencies of single and stacked FZPs at two different incident energies, as well as single and combined structure height of FZPs and optimum FZP structure heights for both incident energies. FZPs are identified as upstream zone plate (USZP), center zone plate (CZP), and downstream zone plate (DSZP). For an evaluation of these values, the optimum structure height for a FZP for the respective incident energies as well as the (combined) structure height for single and stacked FZPs are given. Vertical focus size for 11.8 keV is given as FWHM of line scans over a chromium knife edge.

| | total height | 10 keV (T) | 10 keV (M) | 11.8 keV (T) | 11.8 keV (M) | focus at 11.8 keV |
|---|---|---|---|---|---|---|
| optimum FZP height | | | 1.99 $\mu m$ | | 2.55 $\mu m$ | |
| USZP | 0.8 $\mu m$ | 12.1 % | 9.3 % | 8.0 % | 6.9 % | 210 $nm$ |
| CZP | 0.8 $\mu m$ | 12.1 % | 10.6 % | 8.0 % | 7.7 % | 220 $nm$ |
| DSZP | 0.9 $\mu m$ | 14.6 % | 13.8 % | 9.9 % | 9.6 % | 180 $nm$ |
| USZP & CZP | 1.6 $\mu m$ | 29.9 % | 17.4 % | 23.9 % | 14.3 % | na |
| CZP & DSZP | 1.7 $\mu m$ | 31.2 % | 20.2 % | 25.8 % | 19.4 % | na |
| DSZP & CZP & DSZP | 2.5 $\mu m$ | 28.1% | 18.5 % | 33.8 % | 23.6 % | 220 $nm$ |

Table 2. Theoretical (T) and measured (M) values for FZP efficiencies of single and stacked FZPs at 25 keV.

| | total height | 25 keV (T) | 25 keV (M) | vertical focus size |
|---|---|---|---|---|
| optimum FZP height | | 4.66 $\mu m$ | | |
| FZP1 | 0.8 $\mu m$ | 2.6 % | 2.4 % | 350 $nm$ |
| FZPs1-2 | 1.6 $\mu m$ | 9.4 % | 6.3 % | 350 $nm$ |
| FZPs1-3 | 2.4 $\mu m$ | 18.2 % | 12.6 % | 350 $nm$ |
| FZPs1-4 | 3.2 $\mu m$ | 26.2 % | 16.9 % | 360 $nm$ |
| FZPs1-5 | 4.0 $\mu m$ | 32.2 % | 19.0 % | 390 $nm$ |

tance of approximately 40 $\mu m$, our intermediate-field stack of zone plates had a total distance of 1 $mm$ at 10 keV and 3.25 $mm$ at 25 keV. As this large range allowed for stacking of multiple zone plates, we could overcome previous limitations and mechanically stack up to five FZPs, which resulted in an 8-fold increase of efficiency compared to a single zone plate at 25 keV. This first experimental investigation on intermediate-field stacking of FZPs covered efficiency, misalignment and focus spot size considerations and compared to expectations based on theoretical values or simulations. The measurements confirmed maximum focusing efficiencies at optimum zone heights for respective incident energies. Decrease of focused flux due to either lateral or longitudinal misalignment within the stack of FZPs also followed theoretical progression. The focus spot size was found constant for single and stacked FZPs.

This work was performed by custom designed and built zone plate stacking apparatuses, allowing for straight-forward stacking of multiple zone plates to the zone plate thickness optimum for the respective incident energy. As the travel range of the stages of the stacking apparatus enables working with arrays of FZPs, dedicated FZP chips also provides the possibility to switch FZPs selecting optimum resolution and diameter settings. Thus, intermediate-field FZP stacking with stacking apparatus provides a versatile way of optimizing the illumination based on FZP in a hard X-ray set up for varying focus spot size requirements and a wide range of incident energy. High focusing efficiencies with FZPs at high energies of up to 25 keV have been demonstrated, now enabling high resolution focusing in this hard X-ray regime, potentially including higher energies.

#212663 - $15.00 USD Received 5 Jun 2014; revised 8 Aug 2014; accepted 13 Aug 2014; published 5 Nov 2014

**Acknowledgments**

We would like to acknowledge Liliana Stan, Leonidas E. Ocola and Ed Wrobel with their assistance during the research presented. Data was collected on beamlines 2-ID-D and 2-ID-E at the Advanced Photon Source, Argonne National Laboratory. Use of the Advanced Photon Source, an Office of Science User Facility operated for the U.S. Department of Energy (DOE) Office of Science by Argonne National Laboratory, and Center for Nanoscale Materials was supported by the U.S. DOE under Contract No. DE-AC02-06CH11357.

#212663 - $15.00 USD Received 5 Jun 2014; revised 8 Aug 2014; accepted 13 Aug 2014; published 5 Nov 2014